Inhomogeneous polarization transformation revealing a $\mathcal{PT}$ transition in non-Hermitian optical beam shifts

Niladri Modak,[1,2,*] Swain Ashutosh,[1,3] Shyamal Guchhait,[1] Sayan Ghosh,[1] Ritwik Dhara,[1] Jeeban Kumar Nayak,[1] Sourin Das,[1] and Nirmalya Ghosh[1,†]

[1]*Department of Physical Sciences, Indian Institute of Science Education and Research (IISER) Kolkata, Mohanpur 741246, India*

[2]*Photonics Laboratory, Physics Unit, Tampere University, Tampere 33720, Finland*

[3]*School of Physics and Astronomy, University of Glasgow, Glasgow G12 8QQ, United Kingdom*

(Received 20 June 2024; accepted 15 August 2024; published 27 August 2024)

Despite its non-Hermitian nature, the optical beam shift exhibits real eigenvalues and nonorthogonal eigenstates. To explore this unexpected similarity to typical $\mathcal{PT}$ (parity-time)-symmetric systems, we first categorize the entire parametric regime of optical beam shifts into Hermitian, $\mathcal{PT}$-unbroken, and $\mathcal{PT}$-broken phases. Besides experimentally unveiling the $\mathcal{PT}$-broken regime, crucially, we illustrate that the observed $\mathcal{PT}$ transition is rooted in the momentum-domain inhomogeneous polarization transformation of the beam. The correspondence with a typical non-Hermitian photonic system is further established. Our work not only resolves a fundamental issue in the field of optical beam shift but also puts forward the notion of non-Hermitian spin-orbit photonics: a new direction to study non-Hermitian physics through optical beam shifts.

DOI: 10.1103/PhysRevA.110.023528

I. INTRODUCTION

Optical beam shifts from dielectric interfaces have played an important role in enriching our understanding of various light-matter interactions [1], simulating and interpreting analogous physical phenomena [2,3], and also producing optical devices for metrology and sensing [4]. There are different platforms that exhibit such beam shifts starting from natural light-matter interactions [5], e.g., partial reflection (PR) [5], total internal reflection (TIR) [5], transmission from an interface [5], or through a tilted anisotropic medium [6,7] to exotic metastructures [8]. The longitudinal shift is called Goos-Hänchen (GH) shift [5] and originates from the dispersion of dynamical parameters, e.g., Fresnel coefficients [5] or anisotropic transmission coefficients [6]. The transverse shift is called Imbert-Fedorov (IF) shift or spin-Hall shift [5,9]. It is associated with more intriguing physical phenomena involving the evolution of the geometric phase [5] and the spin-orbit interaction of light [9].

These optical beam shifts are often described by shift matrices [10,11], also known as the Artman operators [10], whose eigenvalue corresponds to the magnitude of the beam shifts [11]. In general, the shift matrices can be non-Hermitian [10,11], and depending on the system parameters, these show some peculiarities. For example, although for TIR the shift matrix is Hermitian, as one goes from TIR to PR, interestingly, the IF shift matrix changes its Hermiticity [5,10]. Moreover, for PR, even though the shift matrix remains non-Hermitian, the eigenvalues can still be real, identical to a $\mathcal{PT}$ (parity-time) symmetric non-Hermitian system, which was previously alluded to in Ref. [11]. On the other hand, the non-Hermitian GH shift matrix does not exhibit such a transition (see Appendix A for details). Although the optical beam shifts have been studied extensively for the last two decades [2,5,6,9–13], such peculiar non-Hermitian nature and its origin remain largely unexplored. Moreover, the optical beam shifts rooted in the straightforward diffractive corrections of the beam [5] exhibiting such strong analogies with intricate $\mathcal{PT}$-symmetric non-Hermitian systems also demand a deeper understanding of its origin. In this work, we address this issue by taking an example of IF shift from reflection of a fundamental Gaussian beam. All the explanations and discussions can be trivially extrapolated for all other polarization-dependent beam shifts (e.g., GH shift) in different light-matter interactions due to their common origin in the momentum or position-domain polarization modulation of the beam [5,8,10].

We first segregate the whole parametric regime into Hermitian, $\mathcal{PT}$-unbroken, and $\mathcal{PT}$-broken phases of IF shifts. We then experimentally detect the momentum-domain eigenshifts in the $\mathcal{PT}$-broken regime, which was not explored earlier. Next and more importantly, we find the origin of the discussed non-Hermiticity in the momentum-domain polarization evolution of the beam and demonstrate that the observed $\mathcal{PT}$ transition [14–16] stems from the momentum-domain inhomogeneous polarization [17] modulation. This way, we not only establish the previously indicated connection of $\mathcal{PT}$ symmetry with optical beam shifts [11] but also lay down a foundation to study the physics of $\mathcal{PT}$ symmetry in the realm of optical beam shifts. Moreover, our calculation reveals that such $\mathcal{PT}$-symmetry physics and $\mathcal{PT}$ transition are not limited to the IF shift operator; instead, it occurs for a similar inhomogeneous polarization element for all possible polarization anisotropy effects.

*Contact author: niladri.modak@tuni.fi

†Contact author: nghosh@iiserkol.ac.in

Note that the $\mathcal{PT}$-symmetric system has recently found great interest in various areas ranging from condensed matter physics [18], optics [19–21], and photonics [22] to material science and engineering [23], especially in the context of non-Hermitian systems. Earlier, losses in physical systems were perceived as undesirable, and measures were taken to avoid them. This is where the alliance between $\mathcal{PT}$ symmetry and non-Hermitian systems offers a great advantage in using or, more so, tuning the loss for various applications [24–26]. Here, we also develop a correspondence with a typical non-Hermitian photonic system, where equal and opposite polarities of pristine spin-Hall shift mimic the two coupled modes with linear polarization-dependent losses representing the coupling. This way, we found that all the signatures of a typical $\mathcal{PT}$-symmetric system can be thoroughly adapted to the optical beam shifts platform. More importantly, unlike other photonic platforms [27], optical beam shifts offer a relatively straightforward platform to model the physics of $\mathcal{PT}$-symmetric non-Hermitian systems through the partial reflection of a Gaussian beam. Therefore, our study not only tackles a fundamental issue in the field of optical beam shift but also puts forward an effective prototype for investigating typical non-Hermitian systems.

II. HERMITICITY OF IF SHIFT IN DIFFERENT PARAMETRIC REGIMES

We start with the well-known shift matrix of the IF shift in the reflection of a light beam with wave number k [10,11].

$$\hat{A}_y = i\frac{\cot\theta}{k}\begin{pmatrix} 0 & (1+r_p/r_s) \\ -(1+r_s/r_p) & 0 \end{pmatrix}. \tag{1}$$

Here, r_p and r_s are the Fresnel reflection coefficients [28] for longitudinal ($\hat{x}$) and transverse ($\hat{y}$) polarized incident light, respectively, and θ is the angle of incidence. The shift matrix acts as the Hamiltonian for the evolution of polarization in the transverse momentum k_y space, resulting in the polarization-dependent IF shift [10]. The matrix $\hat{A}_y$ is, in general, non-Hermitian with eigenvalues $\lambda_\pm$ and eigenstates (right) $|\pm\rangle$ [11],

$$\lambda_\pm = \pm\cot\theta/k(\sqrt{r_p/r_s}+\sqrt{r_s/r_p}),\ |\pm\rangle \sim \begin{pmatrix}\sqrt{r_p}\\ \pm i\sqrt{r_s}\end{pmatrix}. \tag{2}$$

Importantly, when the polarization of the incident beam matches with the $|\pm\rangle$, the magnitude of the IF shift, corresponding to the eigenvalues, becomes the maximum. Note that the real (imaginary) eigenvalues of $\hat{A}_y$ give rise to phase (amplitude) gradient in k_y, which manifests as shifts in y (k_y)-space, producing spatial (angular) beam deflections [10,11]. Now we examine the behavior of $\hat{A}_y$, $\lambda_\pm$, and $|\pm\rangle$ with changing system parameters r_p, r_s, and θ.

In the case of TIR ($\theta >$ the critical angle θ_c), the Fresnel reflection coefficients consist of only phase factors $r_p^{\rm TIR} = e^{i\delta_p}$, $r_s^{\rm TIR} = e^{i\delta_s}$, with $\delta_p - \delta_s = \delta$ [1]. In this case, $\hat{A}_y^{\rm TIR}$ is Hermitian and takes the form $-\cot\theta/k[(1+\cos\delta)\hat{\sigma}_y + \sin\delta\hat{\sigma}_x]$, where $\hat{\sigma}_i$, $i = x, y, z$ are the standard Pauli matrices [12,29]. The eigenvalues are real $\lambda_\pm^{\rm TIR} = \pm 2\frac{\cot\theta}{k}\cos(\delta/2)$, indicating a spatial shift [Figs. 1(a) and 1(b)], and

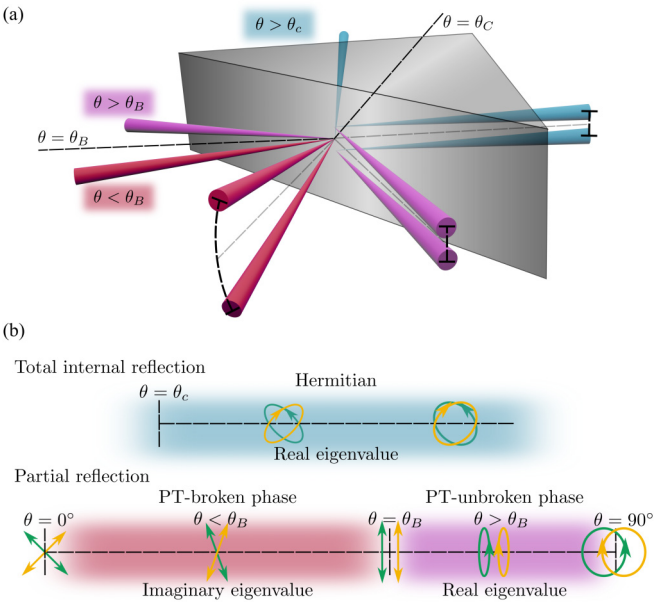

FIG. 1. Schematic illustration of (a) transverse optical beam shifts and (b) the nature of corresponding eigenvalues and eigenstates in different experimental regimes. For TIR, i.e., $\theta > \theta_c$ [blue beams in (a)], the shift is spatial owing to the real eigenvalues of the corresponding Hermitian shift matrix [blue-shaded area in (b)]. The corresponding eigenstates are elliptic and orthogonal (green and yellow ellipses). For PR, the corresponding non-Hermitian shift matrix has real eigenvalues for $\theta > \theta_B$ and imaginary eigenvalues for $\theta < \theta_B$, manifested as spatial [magenta beams in (a)] and momentum-domain shifts [red beams in (a)], respectively. For $\theta > \theta_B$, the nonorthogonal eigenstates are elliptical and become orthogonal circular at $\theta \to 90°$ [magenta-shaded area in (b)]. For $\theta < \theta_B$, the nonorthogonal eigenstates are linear and become orthogonal $\pm 45°$ when $\theta \to 0°$ [magenta-shaded area in (b)]. At $\theta \to \theta_B$, the eigenstates become collinear. The transition in the eigenspectrum around $\theta = \theta_B$ resembles a typical $\mathcal{PT}$-transition, i.e., transition of a non-Hermitian system from $\mathcal{PT}$-unbroken to $\mathcal{PT}$-broken phase.

corresponding eigenstates are elliptic and orthogonal $|\pm\rangle^{\rm TIR} \sim [e^{i\delta/2}\ \pm i]^T$.

However, peculiarity arises for PR as $r_p^{\rm PR}$ and $r_s^{\rm PR}$ are real, and the corresponding shift matrix $\hat{A}_y^{\rm PR}$ is non-Hermitian,

$$\hat{A}_y^{\rm PR} = \frac{\cot\theta}{k}\left[-\left(1+\frac{r_p/r_s + r_s/r_p}{2}\right)\hat{\sigma}_y + i\frac{r_p/r_s - r_s/r_p}{2}\hat{\sigma}_x\right]. \tag{3}$$

Interestingly, Eq. (2) suggests that the eigenvalues and eigenstates of $\hat{A}_y^{\rm PR}$ undergo a transition around $\theta =$ Brewster's angle θ_B [corresponding to $r_p^{\rm PR} = 0$ for a nonmagnetic dielectric interface, e.g., an air-glass interface in Fig. 2(a)] [1,28]. Although $\hat{A}_y^{\rm PR}$ is non-Hermitian, at an angle of incidence $\theta > \theta_B$ ($r_p^{\rm PR} < 0$), the eigenvalues are still real; however, the corresponding eigenstates are nonorthogonal elliptical [11]. On the other hand, at $\theta < \theta_B$ ($r_p^{\rm PR} > 0$), the eigenvalues become imaginary, manifested as a momentum-domain beam shift, and the nonorthogonal eigenstates become linear [Figs. 1(a) and 1(b)]. This change from imaginary to real eigenvalues essentially resembles a typical $\mathcal{PT}$ transition in a non-Hermitian

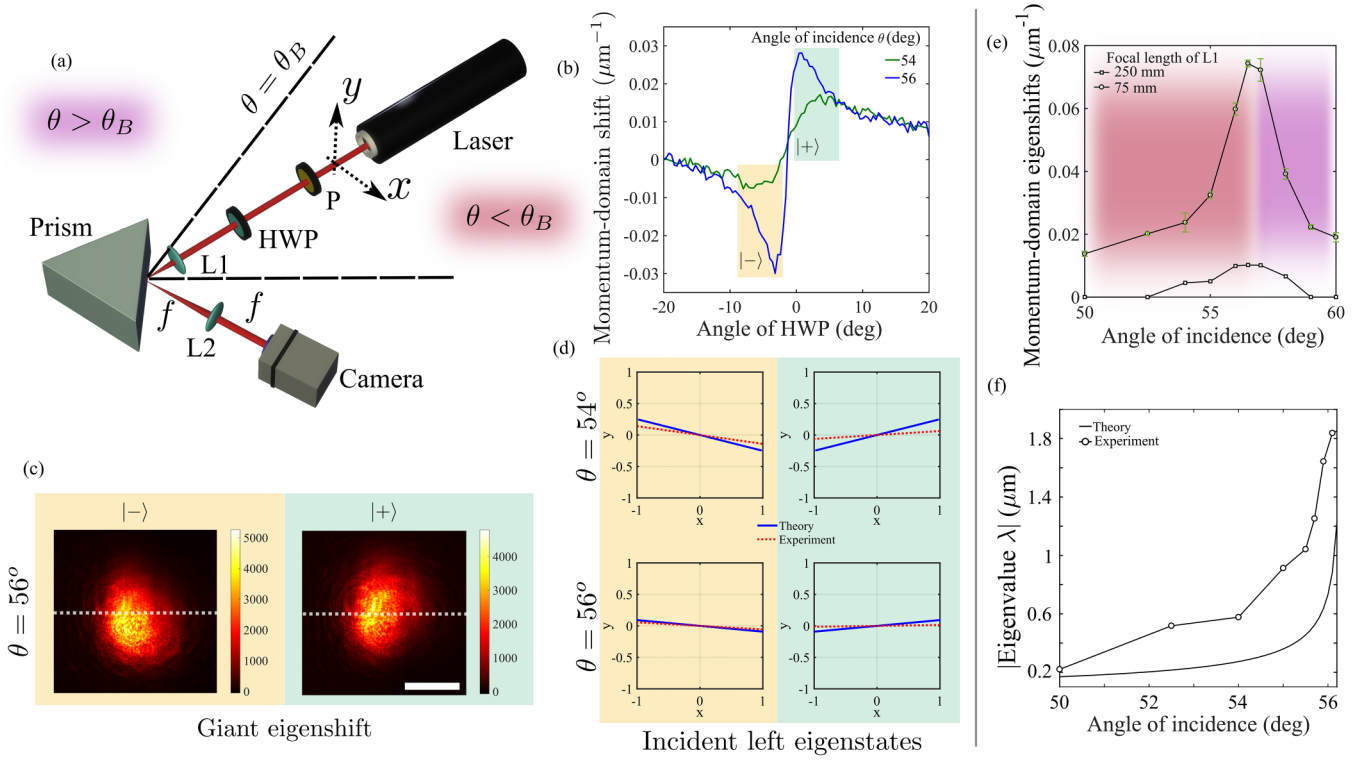

FIG. 2. Experimental detection of momentum-domain giant eigenshifts and extraction of the imaginary eigenvalues at $\theta < \theta_B$. (a) Experimental setup. The laser beam from a He-Ne laser source (633 nm) is partially reflected from a glass prism of refractive index ∼1.5. The focal length of the first lens, L1, is used to tune the spot size of the incident beam to get further control over the magnitude of the momentum-domain eigenshift. The second lens, L2 (focal length 100 mm), is used as a Fourier lens to implement a conventional $2-f$ momentum-space imaging system [30]. (b) Variation of the experimentally observed momentum-domain transverse shift with varying angle of the polarization of the input beam for two representative $\theta = 54^\circ$ (green solid line) and 56° (blue solid line). When the input polarization matches with the left eigenstates $|-\rangle$ (yellow shaded region) and $|+\rangle$ (green shaded region) of $A_y^{\rm PR}$, we get giant shifts, as presented in (c) for $\theta = 56^\circ$. Color bars are intensities in arbitrary units. White scalebar represents a momentum-domain length of ∼0.24 μm^{-1}. (d) The theoretically calculated left eigenstates match well with experimentally determined [from the orientation of the polarizer (P) and half wave plate (HWP)] input polarization state. The states are represented in standard x-y Cartesian space. (e) Variation of the momentum-domain eigenshifts with changing angle of incidence for two different focal lengths of L1: 250 mm (black squares) and 75 mm (black circles). Error bars indicate statistical errors. The color code follows that of Fig. 1. (f) The variation of retrieved eigenvalues (from a larger data set of eigenshifts) with changing angle of incidence for 75 mm focal length of L1 are in agreement with theoretical prediction [Eq. (2)].

system around an "exceptional point" [11,14–16]. This was partly alluded to by Götte and colleagues [11]. Therefore, the demonstration of such transformations in the eigenspectrum of the IF shift matrix in PR mimicking a $\mathcal{PT}$ transition appear to be the first outcome of the present study [Figs. 1(a) and 1(b)]. More importantly, this work reveals the origin of all these transformations, starting from TIR to PR, as we discuss in Sec. IV.

III. EXPERIMENTAL DETECTION OF MOMENTUM-DOMAIN IF SHIFT FOR PARTIAL REFLECTION

Although the spatial shift at $\theta > \theta_B$ has been detected in Ref. [11], the momentum-domain shifts at $\theta < \theta_B$ are still unexplored. We first experimentally detect these shifts. Note that the typical magnitudes of the eigenvalues of $\hat{A}_y^{\rm PR}$ are small. However, the eigenvalues can directly be measured around singular points, e.g., Brewster's angle, where the magnitude of the eigenvalues becomes large [2,11]. A fundamental Gaussian beam from a 633-nm He-Ne Laser is partially reflected from a glass prism [Fig. 2(a)]. To generate the desired linear eigenstates $|\pm\rangle$ in the incident beam, we put a polarizer (P)–half wave plate (HWP) combination [Fig. 2(a)]. Two different focal lengths of L1, 250 mm and 75 mm, are used to tune the spot size of the incident beam and get further control over the magnitude of the momentum-domain eigenshift (see Materials and Methods). The second lens, L2 (focal length 100 mm), is used as a Fourier lens to image the momentum space of the prism plane into the camera. When the input polarization state, by tuning P and HWP, matches with the left eigenstates of $\hat{A}_y^{\rm PR}$ (see Materials and Methods), the momentum-domain shifts become giant [Figs. 2(b) and 2(c)]. The difference in the centroid positions in the momentum domain of the reflected beam for two eigenstates $|\pm\rangle$, i.e., eigenshifts [7], are plotted with changing angle of incidence in Fig. 2(e). Due to the increasing magnitude of the imaginary eigenvalues, the momentum-domain eigenshift increases around Brewster's angle [11,31]. As also evident from Fig. 2(e), the eigenshifts increase significantly with reducing the focal lengths of L1, which is a signature of momentum-domain beam shifts [5,13]. Ideally, the eigenshifts

should be maximum at $\theta = \theta_B$ and fall to zero above θ_B, as the eigenstates are no longer linear in that region. However, in the experimental situation, although the magnitude of such eigenshifts falls rapidly at $\theta > \theta_B$, there is still some appreciable amount of momentum-domain shift. This happens because the incident beam also has a momentum distribution in the longitudinal direction (k_x). Due to this spread, there is always some part of the beam that gets incident at $\theta < \theta_B$ even though the central wave vector of the beam falls at $\theta > \theta_B$. This gives rise to a momentum-domain eigenshift even at $\theta > \theta_B$. The longitudinal spread reduces significantly for the 250-mm focal length of L1. Therefore, the magnitude of the angular eigenshift falls more quickly at $\theta > \theta_B$ in this case; however, the magnitudes of the eigenshifts, in this case, are lower.

The momentum-domain eigenshift Δ and the magnitude of the eigenvalue λ [see Eq. (2)] are connected through the following relation [7]:

$$|\lambda| = \frac{\pi w_0^2}{2\xi f}\Delta. \tag{4}$$

Here, w_0 is the beam waist at focus of L1 on the air-prism interface, ξ is the wavelength of the incident light, and f is the focal length of the Fourier lens, i.e., $f = 100$ mm. Equation (4) is used to retrieve the eigenvalues from experimentally detected eigenshifts Δ in Fig. 2(f). The retrieved eigenvalues agree with the theoretical predictions as noted in Eq. (2) [see Fig. 2(f)]. Error-prone estimation of w_0 [quadratic presence in Eq. (4)] is the cause of the slight mismatch between experimentally retrieved eigenvalues and corresponding theoretical prediction in Eq. (2).

IV. ORIGIN OF ALL THE PECULIARITIES IN THE HERMITICITY OF IF SHIFT

The beam shifts have their origin in the corresponding momentum-domain polarization modulation of the beam [5,10]. The transverse IF shift, specifically, originates from the polarization distribution along the transverse component of momentum (k_y) in the beam [5], and therefore we consider a polarized one-dimensional (1D) Gaussian beam consisting only of k_y. The momentum-space evolution of such a vector beam after TIR or PR is governed by a momentum-domain Jones matrix $\hat{J}(k_y)$. While $\hat{A}_y$ provides the information of these polarization-dependent beam shifts, the corresponding $\hat{J}(k_y)$ consists of all the information of the momentum-domain polarization transformation of the beam exhibiting beam shift. In fact, the shift matrix is conventionally derived from this momentum-domain Jones matrix $\hat{J}(k_y)$ [10,11], i.e.,

$$\begin{pmatrix} r_p & \frac{-k_y\cot\theta}{k}(r_p + r_s) \\ \frac{k_y\cot\theta}{k}(r_p + r_s) & r_s \end{pmatrix} \sim e^{-ik_y\hat{A}_y}\begin{pmatrix} r_p & 0 \\ 0 & r_s \end{pmatrix}. \tag{5}$$

Here, $\left(\begin{smallmatrix} r_p & 0 \\ 0 & r_s \end{smallmatrix}\right)$ is the zeroth-order Fresnel reflection matrix [10,11], and the diffractive corrections of the beam lead to the correction term $\hat{J}_c(k_y) = e^{-ik_y\hat{A}_y}$ responsible for the beam shift. The real and imaginary eigenvalues of $\hat{A}_y$, therefore, result in the spatial and angular shift of the beam, respectively [11].

Note that $\hat{A}_y$ acts as the corresponding differential Jones matrix of $\hat{J}_c(k_y)$ [32,33]. Although the conventional Jones algebra has been extensively used in polarization optics [28], its differential formalism is less noticed [32]. However, differential Jones matrix formalism is quite profound, particularly due to its structural analogy with Schrödinger's formalism of quantum mechanics [29,32].

The eigenvalues of $\hat{J}_c(k_y)$ are

$$\Lambda_\pm = e^{-ik_y(\pm\lambda)}, \text{ with eigenstates} |\pm\rangle. \tag{6}$$

It is well known that the phase and amplitude eigenvalues of a Jones matrix are associated with polarization retardance (unitary) and diattenuation (nonunitary) effect [28]. Moreover, it is apparent from Eqs. (2) and (6) that the k_y-dependent phase and amplitude eigenvalues of $\hat{J}_c(k_y)$ correspond to the real and imaginary eigenvalues of $\hat{A}_y$. The eigenstates of both $\hat{A}_y$ and $\hat{J}_c(k_y)$ are also the same. Hence, real and imaginary eigenvalues of $\hat{A}_y$ are manifestations of momentum-domain polarization retardance [phase eigenvalues of $\hat{J}_c(k_y)$7 and diattenuation [amplitude eigenvalues of $\hat{J}_c(k_y)$] effects, respectively. This one-to-one correspondence between the eigenspectrums of $\hat{J}_c(k_y)$ and $\hat{A}_y$ allows us to use the polarization property of $\hat{J}_c(k_y)$ to understand the physical origin of all the transformations in the eigenspectrum $\hat{A}_y$.

For TIR, the Jones matrix $\hat{J}_c^{\rm TIR}(k_y)$ indicates a simultaneous presence of two unitary systems—circular and $\pm 45^\circ$ linear retarder [32,33] in the momentum domain of the beam [Fig. 3(a)]; $\hat{J}_c^{\rm TIR}(k_y)$ [see Appendix B] is, therefore, unitary and has phase eigenvalues $\Lambda_\pm^{\rm TIR} = e^{-ik_y(\pm\lambda^{\rm TIR})}$ with orthogonal elliptic eigenvectors $|\pm\rangle^{\rm TIR}$. The corresponding shift matrix $\hat{A}_y^{\rm TIR}$ is therefore Hermitian, having real eigenvalues $\pm\lambda^{\rm TIR}$.

On the contrary, the shift matrix for partial reflection $\hat{A}_y^{\rm PR}$ is non-Hermitian, and can be written as an imaginary combination of $\hat{\sigma}_y$ and $\hat{\sigma}_x$, as mentioned earlier. $i\hat{\sigma}_x$ is the differential matrix for a $\pm 45^\circ$ linear diattenuator (nonunitary) [32,33]. Such a simultaneous presence of circular(linear) retarder and linear(circular) diattenuater mimics an inhomogeneous polarization anisotropy element [17] (see Appendix C for details) in the momentum (k_y) domain. Note that nonorthogonal eigenstates (like $|\pm\rangle$) are one of the signatures of inhomogeneous polarization elements [17]. Now we discuss how an inhomogeneous polarization element with the differential matrix $a\hat{\sigma}_y + ib\hat{\sigma}_x$ (a, b are real) behaves under different conditions on the relative magnitude of a and b.

(1) It acts as a diattenuating retarder at $a^2 > b^2$ (see Appendix B), where the retardance effect dominates. Even though the differential matrix is non-Hermitian and the corresponding exponential Jones matrix is nonunitary [32,33], it still has phase eigenvalues. The corresponding eigenstates are nonorthogonal elliptic [Fig. 3(a)].

(2) At $a^2 < b^2$, however, the Jones matrix has amplitude eigenvalues, and eigenstates become nonorthogonal linear (see Appendix B). Amplitude eigenvalues indicate that the system converts into a retarding diattenuater [Fig. 3(a)] [32,33]. In this case, the diattenuation dominates.

(3) At $a^2 = b^2$, the diattenuation and retardance effects contribute equally and give rise to the maximally

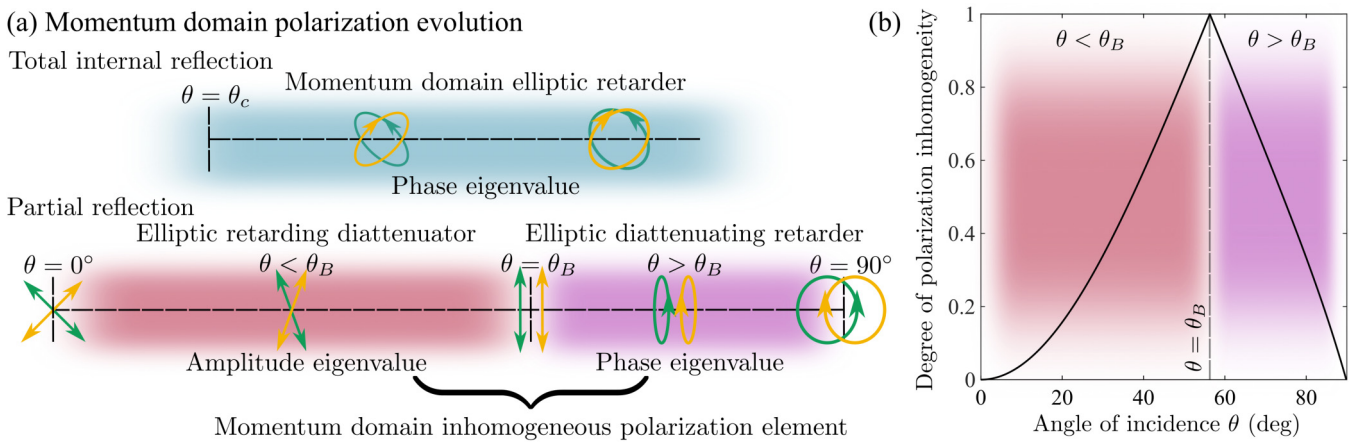

FIG. 3. Momentum-domain polarization transformation is the origin of the discussed characteristics of the eigenspectrum [noted in Fig. 1(b)] of transverse optical beam shift. (a) For TIR, the system acts as a momentum-domain elliptic retarder. In PR, the system acts as a momentum-domain inhomogeneous polarization element, transforming from diattenuating retarder to retarding diattenuator around $\theta = \theta_B$. The eigenstates of all the mentioned momentum-domain polarization elements are the same as the corresponding beam shift operator [see Fig. 1(b) and Eq. (6)]. (b) Variation of the degree of polarization inhomogeneity for partial reflection of a beam from an air-glass (refractive index = 1.5) interface. Brewster's angle ($\theta = \theta_B = 56.31°$) corresponds to the maximum degree of inhomogeneity. The color code follows that of Fig. 1.

inhomogeneous polarization element where the eigenstates of the corresponding Jones matrix become collinear [Fig. 3(a)].

Additionally, we observe that such a transition in the eigenspectrum of the Jones matrix is general for an inhomogeneous polarization element with simultaneous retardance and diattenuation (moreover, for an imaginary combination of Pauli matrices; Appendix D).

As mentioned above, the IF shift in partial reflection is a natural manifestation of such an inhomogeneous polarization anisotropy element in the momentum domain. At an angle of incidence $\theta > \theta_B$, $\hat{J}_c^{\rm PR}(k_y)$ (see Appendix B) has phase eigenvalues resulting in real eigenvalues of $\hat{A}_y^{\rm PR}$ with nonorthogonal elliptic eigenstates $|\pm\rangle^{\rm PR}$ [Eq. (6)]. Therefore, the spatial IF shift in partial reflection for $\theta > \theta_B$ (equivalent to Case 1 above) manifests a momentum-domain elliptic diattenuating retarder [Fig. 3(a)]. For $\theta < \theta_B$, $\hat{J}_c^{\rm PR}(k_y)$ has amplitude eigenvalues resulting in imaginary eigenvalues of $\hat{A}_y^{\rm PR}$ with nonorthogonal linear eigenstates [Eq. (6), see Appendix B]. Therefore, the spatial IF shift in partial reflection for $\theta < \theta_B$ (Case 2) is the manifestation of the momentum-domain elliptic retarding diattenuator. At $\theta = \theta_B$ (Case 3), the eigenstates become collinear, manifesting the maximum degree of inhomogeneity [17]. The variation of the degree of inhomogeneity $1 - |r_p^{\rm PR}/r_s^{\rm PR}|$ (see Appendix C) with changing the angle of incidence is plotted in Fig. 3(b). The momentum-domain polarization transformation becomes maximally inhomogeneous when $\theta \to \theta_B$ and acts as a homogeneous polarization element when $\theta \to 0°,\ 90°$. Therefore, it can be concluded that such transition in the eigenspectrum of the transverse IF shift matrix is a manifestation of the corresponding momentum-domain inhomogeneous polarization transformation.

Note that all such polarization-dependent optical beam shifts are essentially rooted in the momentum or space-domain polarization transformation of the beam [5,8,10]. We considered the IF shift in one of the simplest light-matter interactions, i.e., partial reflection of a fundamental Gaussian beam. However, all the above-mentioned discussions can be trivially extrapolated for all other complex situations.

V. $\mathcal{PT}$-UNBROKEN AND $\mathcal{PT}$-BROKEN PHASES OF IF SHIFT

The Jones matrix $\hat{J}_c^{\rm PR}(k_y) = e^{-ik_y\hat{A}_y^{\rm PR}}$ denotes a k_y evolution of the input polarization state with $\hat{A}_y^{\rm PR}$ being the corresponding evolution Hamiltonian. Such a non-Hermitian Hamiltonian $(a\hat{\sigma}_y + ib\hat{\sigma}_x)$ in the form of a complex combination of different Pauli matrices are, in general, $\mathcal{PT}$ symmetric [11,34,35] (see Appendix E). At $a^2 > b^2$, this Hamiltonian is in the $\mathcal{PT}$-symmetric phase and has real eigenvalues [14–16,27]. This situation corresponds to $\theta > \theta_B$ in the case of $\hat{A}_y^{\rm PR}$. On the other hand, $a^2 < b^2$ is the corresponding $\mathcal{PT}$-broken phase where eigenvalues are imaginary [14–16,27]. In the case of $\hat{A}_y^{\rm PR}$, this situation arises at $\theta < \theta_B$. Therefore, the transition from $\mathcal{PT}$-symmetric to $\mathcal{PT}$-broken phase appears at $a^2 = b^2$, corresponding to $\theta \to \theta_B$ for $\hat{A}_y^{\rm PR}$. A general diattenuator-retarder inhomogeneous polarization element and transverse IF shifts both exhibit such $\mathcal{PT}$ transition, as both the systems are represented by similar imaginary combinations of Pauli matrices (see Appendixes D and E). We further note that the shift matrix $\hat{A}_y^{\rm PR}$ [Eq. (3)], in circular basis, i.e., in the eigenbasis of $\hat{\sigma}_y$, holds a similar form to a conventional $\mathcal{PT}$-symmetric Hamiltonian of photonic modes [14–16,27],

$$\hat{A}_y^{\rm PR} = a\hat{\sigma}_z + ib\hat{\sigma}_y. \tag{7}$$

As apparent from the structure of $\hat{A}_y^{\rm PR}$ in Eq. (7), the equal and opposite polarities of pristine spin-Hall shift $\pm a$ with left and right circular polarization eigenstates mimic the two coupled systems. b, comprising linear polarization-dependent losses (the unequal magnitude of $r_p^{\rm PR}$ and $r_s^{\rm PR}$ during partial reflection) in the momentum domain, provides the coupling between the two spin-Hall modes. This hybridization leads to new sets of eigenvectors, i.e., generally elliptical polarization

states, which may not be orthogonal. Thus, the parameter b can be identified as the coupling coefficient in the usual scenario of resonant systems having gain and loss [14–16,27]. At $r_p^{\rm PR} = r_s^{\rm PR}$ ($\theta \to 90^\circ$), the shifts become purely spin-Hall analogous to an uncoupled resonant system with real eigenvalue. This is also consistent with the physical origin of the spin-Hall shift [5]. The spin-Hall shift originates from the equal and opposite magnitude of the momentum-domain geometric phase gradient for input left and right circular polarization [5]. Linear polarization-dependent reflectivities, i.e., $r_p^{\rm PR}$ and $r_s^{\rm PR}$, generate an asymmetry of geometric phase gradient between circular polarization states [5]. It is apparent that when the coupling is small ($a^2 > b^2$), although the eigenstates become nonorthogonal, the pristine spin-Hall system dominates and gives real eigenvalues. However, at $a^2 < b^2$, the coupling dominates, providing imaginary eigenvalues. Although the transition from real to imaginary eigenvalues happens around Brewster's angle ($a^2 = b^2$) at the same time, one cannot go arbitrarily close to such a singular point, i.e., $r_p^{\rm PR} = 0$ (in our system), as the exponentiation of $\hat{A}_y^{\rm PR}$ cannot be done there [Eq. (5)]. However, it should be noted that in practice, the magnitude of the beam shift at $\theta = \theta_B$ takes finite value [31], as also apparent from Fig. 2(e). Therefore, the richer physics of the non-Hermitian systems is built in a simple partial reflection of a Gaussian beam.

VI. DISCUSSION: NON-HERMITIAN SPIN-ORBIT PHOTONICS

We demonstrate that the observed $\mathcal{PT}$ transition, and consequently the existence of real eigenvalues, in non-Hermitian IF shift originates from the momentum-domain inhomogeneous polarization transformation of the beam. We characterize the entire parameter space of the IF shift by demarcating the Hermitian, $\mathcal{PT}$-unbroken, and $\mathcal{PT}$-broken regimes. We probe the previously unexplored $\mathcal{PT}$-broken regime of the IF shift by experimentally detecting the momentum-domain giant eigenshifts. More importantly, the description involving momentum-domain inhomogeneous polarization transformation can be generalized to all such polarization-dependent beam shifts occurring in different light-matter interactions. Although this work encompasses the fundamental physics of $\mathcal{PT}$ symmetry in optical beam shifts, there remain gaps that invite further investigation. Specifically, the connection between Brewster's angle and exceptional points is not firmly established, as our model cannot approach Brewster's angle arbitrarily closely. Consequently, a comprehensive theoretical model could be developed in the future to integrate the intriguing physics of exceptional points into the relatively simple platforms of optical beam shifts.

Besides resolving the above-mentioned fundamental issue of non-Hermitan optical beam shifts, the present study yields some important consequences, as mentioned below. The IF shift matrix and the differential matrix of inhomogeneous polarization elements are both modeled through similar imaginary combinations of Pauli matrices that incorporate non-Hermitian physics and exhibit $\mathcal{PT}$ transition. In the context of the former, the momentum-domain polarization modulation, described by $\hat{J}_c(k_y)$, is generally related to the geometric phase evolution and spin-orbit interaction of light already demonstrated in a wide variety of optical systems and metamaterials [5,6,36–38]. However, in dealing with such spin-orbit effects, the polarization-dependent losses are usually ignored. Yet in practice, such losses are inherent, which make the system non-Hermitian [5,6,36–38]. Our study provides a framework for designing controllable non-Hermitian spin-orbit optical materials by including and, moreover, tailoring such polarization-dependent losses. The latter indicates that $\mathcal{PT}$-symmetric non-Hermitian systems can be constructed using regular polarization optical elements (anisotropic materials) by suitably mixing the diattenuation (polarization-dependent losses) and retardance (polarization-dependent phase modifications) effects [17,39]. Hence, this work presents substantial fundamental advancement in understanding optical beam shift, opens up new directions in the study of non-Hermitian systems, and provides simple platforms of optical beam shifts to realize and investigate inherent physics.

VII. MATERIALS AND METHODS

Experimental detection of momentum-domain eigenshifts

We experimentally detect the momentum-domain eigenshifts corresponding to the imaginary eigenvalue of $A_y^{\rm PR}$. We put a Glan-Thompson polarizer P (GTH10M-A, ThorLabs, USA), half wave plate HWP (WPH10M-633, Thorlabs, USA) combination [Fig. 2(a)] fixed at a motorized precision rotation mount (KPRM1E/M, Thorlabs, USA) to generate the desired eigenstates in the incident light. The glass prism is mounted on a precision rotation base (HDR50/M, ThorLabs, USA) to precisely control the angle of incidence. Since $\hat{A}_y$ is a non-Hermitian matrix, one can distinguish between its right and left eigenstates. The right and the left eigenstates are $\begin{pmatrix} \sqrt{r_p} \\ \pm i\sqrt{r_s} \end{pmatrix}$ and $\begin{pmatrix} \sqrt{r_s} \\ \pm i\sqrt{r_p} \end{pmatrix}$, respectively. To get the right eigenstate as input polarization, we have to prepare the left eigenstate using P and HWP combinations [7,11]. For 250 mm focal length (LB1056, Thorlabs, USA), we get a bigger beam waist at focus; for 75 mm focal length (LB1901, Thorlabs, USA), we get a smaller spot size [5]. It is evident from the previous literature [40] that the bigger the beam waist of the incident beam, the smaller the momentum-domain (angular) shift. It is also evident from our experimental results [Fig. 2(e)] that the eigenshifts increase significantly with reducing the focal length of L1.

ACKNOWLEDGMENTS

The authors are grateful for the support of the Indian Institute of Science Education and Research Kolkata (IISER-K), Ministry of Education, Government of India. The authors would like to acknowledge the Science and Engineering Research Board, Government of India, for the funding (Grant No. CRG/2019/005558). We are thankful to Alok Kumar Pan (IIT Hyderabad) for his initial suggestions and discussions. We also want to acknowledge Subhasish Dutta Gupta (TIFR Hyderabad), and Abir Mondal (IISER-K) for scientific discussions that helped to improve our work. R.D. acknowledges Ministry of Education, India, for a PMRF research fellowship grant. S.G. additionally acknowledges CSIR, Government of India, for research fellowships.

APPENDIX A: NON-HERMITIAN LONGITUDINAL GOOS-HÄNCHEN OPTICAL BEAM SHIFT OPERATOR

The longitudinal optical beam shift operator $\begin{pmatrix} -i\frac{\partial \ln r_p}{\partial \theta_i} & 0 \\ 0 & -i\frac{\partial \ln r_s}{\partial \theta_i} \end{pmatrix}$ is Hermitian for total internal reflection (TIR) and non-Hermitian for partial reflection (PR). Similar to Imbert-Fedorov (IF) shift matrix, this non-Hermitian nature can also be understood through the corresponding momentum-domain polarization transformation of the reflected beam [10,11]. While partially reflecting from an interface, different longitudinal wave vectors (k_x) of the incident beam experience different angles of incidence, and therefore, different Fresnel reflection coefficient [5]. Due to this dispersion of longitudinal wave vectors, the beam experiences a momentum-domain polarization transformation [5,10,11]. In the case of TIR, the Fresnel coefficients appear essentially as phase factors [41], and therefore, the polarization modulation becomes a momentum-domain linear retarder. Hence, the corresponding shift matrix is Hermitian with real eigenvalues. On the other hand, for PR, Fresnel coefficients are real and the corresponding polarization modulation becomes a momentum-domain linear diattenuator. The shift matrix, in this case, becomes non-Hermitian with imaginary eigenvalues. The eigenstates of the shift matrix, for TIR [12] and PR, remain orthogonal horizontal and vertical linear polarizations.

APPENDIX B: THE FORM OF $\hat{J}_c(k_y)$ IN TOTAL INTERNAL REFLECTION AND PARTIAL REFLECTION

For TIR,

$$\hat{J}_c^{\mathrm{TIR}}(k_y) = \begin{pmatrix} \cos\left(\frac{2k_y \cot\theta}{k}\cos\delta/2\right) & \frac{(e^{i\delta}+1)}{\sqrt{2(1+\cos\delta)}}\sin\left(\frac{2k_y\cot\theta}{k}\cos\delta/2\right) \\ -\frac{(e^{i\delta}+1)}{\sqrt{2(1+\cos\delta)}}\sin\left(\frac{2k_y\cot\theta}{k}\cos\delta/2\right) & \cos\left(\frac{2k_y\cot\theta}{k}\cos\delta/2\right) \end{pmatrix}. \tag{B1}$$

All the parameters in Eq. (B1) are defined in the main text. Straightforward calculation shows that the eigenvalues and eigenstates of $\hat{J}_c^{\mathrm{TIR}}(k_y)$, respectively, are $\Lambda_\pm^{\mathrm{TIR}} = e^{\mp 2i\frac{k_y\cot\theta}{k}\cos(\delta/2)}$, $|\pm\rangle^{\mathrm{TIR}} \sim [e^{i\delta/2} \ \pm i]^T$.

For PR, at $\theta > \theta_B$,

$$\hat{J}_c^{\mathrm{PR}}(k_y) = \begin{pmatrix} \cos\left[\frac{k_y\cot\theta}{k}\left(\sqrt{\left|\frac{r_p}{r_s}\right|}+\sqrt{\left|\frac{r_s}{r_p}\right|}\right)\right] & \sqrt{\left|\frac{r_p}{r_s}\right|}\sin\left[\frac{\cot k_y\theta}{k}\left(\sqrt{\left|\frac{r_p}{r_s}\right|}+\sqrt{\left|\frac{r_s}{r_p}\right|}\right)\right] \\ -\sqrt{\left|\frac{r_s}{r_p}\right|}\sin\left[\frac{k_y\cot\theta}{k}\left(\sqrt{\left|\frac{r_p}{r_s}\right|}+\sqrt{\left|\frac{r_s}{r_p}\right|}\right)\right] & \cos\left[\frac{k_y\cot\theta}{k}\left(\sqrt{\left|\frac{r_p}{r_s}\right|}+\sqrt{\left|\frac{r_s}{r_p}\right|}\right)\right] \end{pmatrix}. \tag{B2}$$

The eigenvalues and eigenstates, in this case, are $\Lambda_\pm = e^{\mp ik_y\cot\theta/k(\sqrt{|r_p/r_s|}+\sqrt{|r_s/r_p|})}$, $|\pm\rangle \sim [\sqrt{|r_p|} \ \pm i\sqrt{|r_s|}]^T$.

For partial reflection, at $\theta < \theta_B$,

$$\hat{J}_c^{\mathrm{PR}}(k_y) = \begin{pmatrix} \cosh\left[\frac{k_y\cot\theta}{k}\left(\sqrt{\left|\frac{r_p}{r_s}\right|}+\sqrt{\left|\frac{r_s}{r_p}\right|}\right)\right] & -\sqrt{\left|\frac{r_p}{r_s}\right|}\sinh\left[\frac{\cot k_y\theta}{k}\left(\sqrt{\left|\frac{r_p}{r_s}\right|}+\sqrt{\left|\frac{r_s}{r_p}\right|}\right)\right] \\ \sqrt{\left|\frac{r_s}{r_p}\right|}\sinh\left[\frac{k_y\cot\theta}{k}\left(\sqrt{\left|\frac{r_p}{r_s}\right|}+\sqrt{\left|\frac{r_s}{r_p}\right|}\right)\right] & \cosh\left[\frac{k_y\cot\theta}{k}\left(\sqrt{\left|\frac{r_p}{r_s}\right|}+\sqrt{\left|\frac{r_s}{r_p}\right|}\right)\right] \end{pmatrix}. \tag{B3}$$

The eigenvalues and eigenstates, in this case, are $\Lambda_\pm = e^{\pm k_y\cot\theta/k(\sqrt{|r_p/r_s|}+\sqrt{|r_s/r_p|})}$, $|\pm\rangle \sim [\sqrt{|r_p|} \ \pm \sqrt{|r_s|}]^T$.

APPENDIX C: INHOMOGENEOUS POLARIZATION ELEMENTS

Polarization elements are usually characterized by the associated polarization anisotropy effects, e.g., linear and circular diattenuation and birefringence [28]. Regular ideal polarization elements, such as polarizers or wave plates, possess single polarization anisotropy effect, i.e., linear diattenuation or retardance, respectively [28]. However, most of the naturally evolving materials come with the simultaneous presence of multiple polarization anisotropy effects [28,39,42–44]. Inhomogeneous polarization elements are those having (a) simultaneous diattenuation and retardance effects (diattenuator-retarder) or (b) different diattenuation effects (diattenuator-diattenuator) with their axes not parallel or perpendicular [17]. In the present study, we limit our discussions only to the diattenuator-retarder inhomogeneous polarization elements only. We consider all possible combinations of such inhomogeneous polarization elements as follows: (1) circular retarder and ±45° linear diattenuator, (2) circular retarder and horizontal-vertical linear diattenuator, (3) horizontal-vertical linear retarder and ±45° linear diattenuator, and (4) ±45° linear retarder and circular diattenuator.

Such inhomogeneous polarization elements are described by the corresponding differential matrices [32], respectively, listed in the first column of Fig. 4. Note that there are two other similar inhomogeneous polarization elements, i.e., simultaneous ±45° linear retarder and horizontal-vertical linear diattenuator, and horizontal-vertical linear retarder and circular diattenuator, which are similar to, respectively, Case 3 and Case 4 above; therefore, their characteristics can be extrapolated from Case 3 and Case 4. The magnitude of retardance is a, and diattenuation is b for all the cases. The corresponding exponential matrices [32,33] are the regular Jones matrices for those inhomogeneous polarization elements.

Unlike homogeneous polarization elements, the eigenstates of the Jones matrices of inhomogeneous polarization elements are nonorthogonal. And, the degree of inhomogeneity is conventionally described by the overlap between two

$a^2 > b^2$

Differential matrix	Exponential matrix	Eigenvalues $\Lambda_\pm$	Eigenstates $\lvert\pm\rangle$
$a\hat{\sigma}_y + ib\hat{\sigma}_x$	$\begin{pmatrix} \cos(\sqrt{a^2-b^2}) & \frac{(b-a)}{\sqrt{a^2-b^2}}\sin(\sqrt{a^2-b^2}) \\ \frac{(a+b)}{\sqrt{a^2-b^2}}\sin(\sqrt{a^2-b^2}) & \cos(\sqrt{a^2-b^2}) \end{pmatrix}$	$e^{\mp i\sqrt{a^2-b^2}}$	$[\mp i\frac{\sqrt{a^2-b^2}}{a+b}\ 1]^T$
$a\hat{\sigma}_y + ib\hat{\sigma}_z$	$\begin{pmatrix} \cos(\sqrt{a^2-b^2}) + \frac{b}{\sqrt{a^2-b^2}}\sin(\sqrt{a^2-b^2}) & \frac{-a}{\sqrt{a^2-b^2}}\sin(\sqrt{a^2-b^2}) \\ \frac{a}{\sqrt{a^2-b^2}}\sin(\sqrt{a^2-b^2}) & \cos(\sqrt{a^2-b^2}) - \frac{b}{\sqrt{a^2-b^2}}\sin(\sqrt{a^2-b^2}) \end{pmatrix}$	$e^{\mp i\sqrt{a^2-b^2}}$	$[\frac{b\mp i\sqrt{a^2-b^2}}{a}\ 1]^T$
$a\hat{\sigma}_z + ib\hat{\sigma}_x$	$\begin{pmatrix} \cos(\sqrt{a^2-b^2}) - \frac{ia}{\sqrt{a^2-b^2}}\sin(\sqrt{a^2-b^2}) & \frac{b}{\sqrt{a^2-b^2}}\sin(\sqrt{a^2-b^2}) \\ \frac{b}{\sqrt{a^2-b^2}}\sin(\sqrt{a^2-b^2}) & \cos(\sqrt{a^2-b^2}) + \frac{ia}{\sqrt{a^2-b^2}}\sin(\sqrt{a^2-b^2}) \end{pmatrix}$	$e^{\pm i\sqrt{a^2-b^2}}$	$[\frac{-ia\pm i\sqrt{a^2-b^2}}{b}\ 1]^T$
$a\hat{\sigma}_x + ib\hat{\sigma}_y$	$\begin{pmatrix} \cos(\sqrt{a^2-b^2}) & \frac{-i(b+a)}{\sqrt{a^2-b^2}}\sin(\sqrt{a^2-b^2}) \\ \frac{i(b-a)}{\sqrt{a^2-b^2}}\sin(\sqrt{a^2-b^2}) & \cos(\sqrt{a^2-b^2}) \end{pmatrix}$	$e^{\pm i\sqrt{a^2-b^2}}$	$[\mp\frac{\sqrt{a^2-b^2}}{a-b}\ 1]^T$

$a^2 < b^2$

Differential matrix	Exponential matrix	Eigenvalues $\Lambda_\pm$	Eigenstates $\lvert\pm\rangle$
$a\hat{\sigma}_y + ib\hat{\sigma}_x$	$\begin{pmatrix} \cosh(\sqrt{b^2-a^2}) & \frac{(b-a)}{\sqrt{b^2-a^2}}\sinh(\sqrt{b^2-a^2}) \\ \frac{(b+a)}{\sqrt{b^2-a^2}}\sinh(\sqrt{b^2-a^2}) & \cosh(\sqrt{b^2-a^2}) \end{pmatrix}$	$e^{\mp\sqrt{b^2-a^2}}$	$[\mp\frac{\sqrt{b^2-a^2}}{a+b}\ 1]^T$
$a\hat{\sigma}_y + ib\hat{\sigma}_z$	$\begin{pmatrix} \cosh(\sqrt{b^2-a^2}) + \frac{b}{\sqrt{b^2-a^2}}\sin(\sqrt{b^2-a^2}) & \frac{-a}{\sqrt{b^2-a^2}}\sinh(\sqrt{b^2-a^2}) \\ \frac{a}{\sqrt{b^2-a^2}}\sinh(\sqrt{b^2-a^2}) & \cosh(\sqrt{b^2-a^2}) - \frac{b}{\sqrt{b^2-a^2}}\sin(\sqrt{b^2-a^2}) \end{pmatrix}$	$e^{\mp\sqrt{b^2-a^2}}$	$[\frac{b\mp\sqrt{b^2-a^2}}{a}\ 1]^T$
$a\hat{\sigma}_z + ib\hat{\sigma}_x$	$\begin{pmatrix} \cosh(\sqrt{b^2-a^2}) - \frac{ia}{\sqrt{b^2-a^2}}\sin(\sqrt{b^2-a^2}) & \frac{b}{\sqrt{b^2-a^2}}\sinh(\sqrt{b^2-a^2}) \\ \frac{b}{\sqrt{b^2-a^2}}\sinh(\sqrt{b^2-a^2}) & \cosh(\sqrt{b^2-a^2}) + \frac{ia}{\sqrt{b^2-a^2}}\sin(\sqrt{b^2-a^2}) \end{pmatrix}$	$e^{\mp\sqrt{b^2-a^2}}$	$[\frac{-ia\mp\sqrt{b^2-a^2}}{b}\ 1]^T$
$a\hat{\sigma}_x + ib\hat{\sigma}_y$	$\begin{pmatrix} \cosh(\sqrt{b^2-a^2}) & \frac{-i(b+a)}{\sqrt{b^2-a^2}}\sinh(\sqrt{b^2-a^2}) \\ \frac{i(b-a)}{\sqrt{b^2-a^2}}\sinh(\sqrt{b^2-a^2}) & \cosh(\sqrt{b^2-a^2}) \end{pmatrix}$	$e^{\mp\sqrt{b^2-a^2}}$	$[\mp i\frac{\sqrt{b^2-a^2}}{a-b}\ 1]^T$

FIG. 4. Phase transition in the eigenvalue spectrum of the Jones matrix of general diattenuator-retarder inhomogeneous polarization elements. The exponential Jones matrices have phase eigenvalues at $a^2 > b^2$, demonstrating a typical diattenuating-retarder inhomogeneous polarization element. On the other hand, they transform to amplitude eigenvalues at $a^2 < b^2$ as the system acts as retarding diattenuator there. The eigenstates tend to be collinear at $a^2 \to b^2$.

eigenstates [17]. Maximum inhomogeneity appears when two eigenstates become parallel (at $a^2 \to b^2$), and the overlap becomes unity. In this limit, the magnitude of diattenuation tends to become equal to the magnitude of retardance.

In our case of partial reflection, the shift matrix resembles the differential matrix of an inhomogeneous polarization element consisting of a simultaneous circular retarder and $\pm 45^\circ$ linear diattenuator. The corresponding momentum-domain Jones matrix $\hat{J}_c^{\mathrm{PR}}(k_y)$ also has nonorthogonal eigenstates. The overlap of the eigenstates, in our case, is $1 - |r_p^{\mathrm{PR}}/r_s^{\mathrm{PR}}|$, which reaches unity at $\theta \to \theta_B$, indicating the maximum degree of inhomogeneity.

APPENDIX D: TRANSITION IN THE EIGENSPECTRUM OF A GENERAL DIATTENUATOR-RETARDER INHOMOGENEOUS POLARIZATION ELEMENT

As discussed in the main text, the shift matrix A_y^{PR} is a complex combination of a circular retarder and a $\pm 45^\circ$ linear diattenuator. In such an inhomogeneous polarization element, the eigenvalues and eigenstates of the corresponding Jones matrix exhibit a phase transition around $a^2 \to b^2$ (see Fig. 4). In a similar manner, we examine the outcomes of all such possible complex combinations of retarder and diattenuator matrices. The Jones matrices, eigenvalues, and eigenstates are noted for all such combinations in Fig. 4.

Differential matrix	P operator	PT-unbroken phase ($a^2 > b^2$)		PT-broken phase ($a^2 < b^2$)	
		Eigenvalues $\lambda_\pm$	Eigenstates $\|\pm\rangle$	Eigenvalues $\lambda_\pm$	Eigenstates $\|\pm\rangle$
$a\hat{\sigma}_y + ib\hat{\sigma}_x$	$\hat{\sigma}_z = \begin{pmatrix} 1 & 0 \\ 0 & -1 \end{pmatrix}$	$\pm\sqrt{a^2-b^2}$	$[\mp i\frac{\sqrt{a^2-b^2}}{a+b}\ 1]^T$	$\mp i\sqrt{b^2-a^2}$	$[\mp\frac{\sqrt{b^2-a^2}}{a+b}\ 1]^T$
$a\hat{\sigma}_y + ib\hat{\sigma}_z$	$\hat{\sigma}_x = \begin{pmatrix} 0 & 1 \\ 1 & 0 \end{pmatrix}$	$\pm\sqrt{a^2-b^2}$	$[\frac{b\mp i\sqrt{a^2-b^2}}{a}\ 1]^T$	$\mp i\sqrt{b^2-a^2}$	$[\frac{b\mp\sqrt{b^2-a^2}}{a}\ 1]^T$
$a\hat{\sigma}_z + ib\hat{\sigma}_x$	$\hat{\sigma}_z = \begin{pmatrix} 1 & 0 \\ 0 & -1 \end{pmatrix}$	$\mp\sqrt{a^2-b^2}$	$[\frac{-ia\pm i\sqrt{a^2-b^2}}{b}\ 1]^T$	$\mp i\sqrt{b^2-a^2}$	$[\frac{-ia\mp\sqrt{b^2-a^2}}{b}\ 1]^T$
$a\hat{\sigma}_x + ib\hat{\sigma}_y$	$\hat{\mathbb{I}} = \begin{pmatrix} 1 & 0 \\ 0 & 1 \end{pmatrix}$	$\mp\sqrt{a^2-b^2}$	$[\mp\frac{\sqrt{a^2-b^2}}{a-b}\ 1]^T$	$\mp i\sqrt{b^2-a^2}$	$[\mp i\frac{\sqrt{b^2-a^2}}{a-b}\ 1]^T$

FIG. 5. $\mathcal{PT}$-unbroken and broken phase for general diattenuator-retarder inhomogeneous polarization elements. The forms of the differential matrices of the polarization elements and corresponding parity ($\mathcal{P}$) operators are listed in the first and second columns, respectively [11,27,34,35]. Eigenvalues of the differential matrices real at $a^2 > b^2$ and corresponding eigenstates are the eigenstates of the $\mathcal{PT}$ operator. This regime is the $\mathcal{PT}$-unbroken phase. At $a^2 < b^2$, the eigenvalues become imaginary, and the eigenstates are not the eigenstates of the $\mathcal{PT}$ operator, indicating the $\mathcal{PT}$-broken phase. The eigenvalues coalesce to zero at $a^2 \to b^2$, and corresponding eigenstates become parallel. Thus, $a^2 = b^2$ acts as an exceptional point.

APPENDIX E: $\mathcal{PT}$ SYMMETRY IN $\hat{A}_y$ FOR PARTIAL REFLECTION

As discussed in the main text, the transverse optical shift matrix for partial reflection $\hat{A}_y^{\mathrm{PR}}$ is non-Hermitian. This non-Hermitian matrix is parity-time ($\mathcal{PT}$) symmetric [11,27,34,35]. The $\mathcal{P}$ operator, in this case, is the third Pauli matrix $\hat{\sigma}_z$. On the other hand, the $\mathcal{T}$ operator is just a complex conjugation [14,16]. At $\theta > \theta_B$, the eigenvalues of $\hat{A}_y^{\mathrm{PR}}$ are real, and corresponding elliptical eigenstates are the eigenstates of the $\mathcal{PT}$ operator. Therefore, $\theta > \theta_B$ is the regime for the $\mathcal{PT}$-unbroken phase. On the contrary, at $\theta < \theta_B$, the eigenvalues are imaginary, and corresponding linear eigenstates are not the eigenstates of the $\mathcal{PT}$ operator, indicating the $\mathcal{PT}$-broken phase.

Note that $\hat{A}_y^{\mathrm{PR}}$ resembles the differential Jones matrix for the circular retarder-$\pm 45^\circ$ linear diattenuator inhomogeneous polarization element (see Appendix C). The differential matrices of all other inhomogeneous polarization elements are also $\mathcal{PT}$ symmetric with the $\mathcal{P}$ operators listed in Fig. 5 and the $\mathcal{T}$ operator to complex conjugation [15]. In all the cases, eigenvalues of the differential matrices are real at $a^2 > b^2$ and corresponding eigenstates are the eigenstates of the $\mathcal{PT}$ operator. This regime is the $\mathcal{PT}$-unbroken phase. At $a^2 < b^2$, the eigenvalues become imaginary, and the eigenstates are not the eigenstates of the $\mathcal{PT}$ operator, indicating the $\mathcal{PT}$-broken phase. The eigenvalues coalesce to zero at $a^2 \to b^2$, and corresponding eigenstates become parallel. Thus, the maximum inhomogeneity situation $a^2 = b^2$ acts as an exceptional point (see Appendix D).

As mentioned earlier, similar transitions also happen around $\theta \to \theta_B$ in the case of partial reflection. The degree of inhomogeneity in the corresponding momentum-domain Jones matrix $\hat{J}_c^{\mathrm{PR}}(k_y)$ goes maximum [see Fig. 3(b) of the main text]. The eigenstates of $\hat{A}_y^{\mathrm{PR}}$ also tend to coalesce; however, the eigenvalues tend to diverge. This happens because the form of $\hat{A}_y^{\mathrm{PR}}$ does not allow us to write it as an imaginary combination of $\hat{\sigma}_x$ and $\hat{\sigma}_y$, and moreover, the first-order approximation to describe the beam shifts becomes invalid, and consequently, the eigenspectrum of $\hat{A}_y^{\mathrm{PR}}$ encounters a singularity.

[1] M. Born and E. Wolf, *Principles of Optics: Electromagnetic Theory of Propagation, Interference and Diffraction of Light* (Elsevier, New York, 2013).

[2] N. Modak, S. Ashutosh, S. Guchhait, S. Das, A. K. Pan, and N. Ghosh, Laser Photonics Rev. **17**, 2300166 (2023).

[3] M. Asano *et al.*, Nat. Commun. **7**, 13488 (2016).

[4] X. Ling, X. Zhou, K. Huang, Y. Liu, C.-W. Qiu, H. Luo, and S. Wen, Rep. Prog. Phys. **80**, 066401 (2017).

[5] K. Y. Bliokh and A. Aiello, J. Opt. **15**, 014001 (2013).

[6] K. Y. Bliokh, C. Samlan, C. Prajapati, G. Puentes, N. K. Viswanathan, and F. Nori, Optica **3**, 1039 (2016).

[7] N. Modak, S. Das, P. Bordoloi, and N. Ghosh, Phys. Rev. A **105**, 033713 (2022).

[8] Q. Kong, H.-Y. Shi, J.-L. Shi, and X. Chen, Opt. Express **27**, 11902 (2019).

[9] O. Hosten and P. Kwiat, Science **319**, 787 (2008).

[10] F. Töppel, M. Ornigotti, and A. Aiello, New J. Phys. **15**, 113059 (2013).
[11] J. B. Götte, W. Löffler, and M. R. Dennis, Phys. Rev. Lett. **112**, 233901 (2014).
[12] G. Jayaswal, G. Mistura, and M. Merano, Opt. Lett. **39**, 2266 (2014).
[13] S. Goswami, M. Pal, A. Nandi, P. K. Panigrahi, and N. Ghosh, Opt. Lett. **39**, 6229 (2014).
[14] C. M. Bender and S. Boettcher, Phys. Rev. Lett. **80**, 5243 (1998).
[15] R. El-Ganainy, K. G. Makris, M. Khajavikhan, Z. H. Musslimani, S. Rotter, and D. N. Christodoulides, Nat. Phys. **14**, 11 (2018).
[16] A. Krasnok, N. Nefedkin, and A. Alu, arXiv:2103.08135.
[17] S.-Y. Lu and R. A. Chipman, J. Opt. Soc. Am. A **11**, 766 (1994).
[18] M. Kreibich, J. Main, H. Cartarius, and G. Wunner, Phys. Rev. A **90**, 033630 (2014).
[19] A. Guo, G. J. Salamo, D. Duchesne, R. Morandotti, M. Volatier-Ravat, V. Aimez, G. A. Siviloglou, and D. N. Christodoulides, Phys. Rev. Lett. **103**, 093902 (2009).
[20] Q. Yue, W. Zhen, Y. Ding, X. Zhou, and D. Deng, Opt. Mater. Express **11**, 3954 (2021).
[21] M. Berry, J. Opt. **13**, 115701 (2011).
[22] J. Doppler, A. A. Mailybaev, J. Böhm, U. Kuhl, A. Girschik, F. Libisch, T. J. Milburn, P. Rabl, N. Moiseyev, and S. Rotter, Nature (London) **537**, 76 (2016).
[23] A. Lupu, H. Benisty, and A. Degiron, Opt. Express **21**, 21651 (2013).
[24] Z. Lin, H. Ramezani, T. Eichelkraut, T. Kottos, H. Cao, and D. N. Christodoulides, Phys. Rev. Lett. **106**, 213901 (2011).
[25] H. Hodaei, M.-A. Miri, M. Heinrich, D. N. Christodoulides, and M. Khajavikhan, Science **346**, 975 (2014).
[26] R. Fleury, D. Sounas, and A. Alù, Nat. Commun. **6**, 5905 (2015).
[27] Ş. K. Özdemir, S. Rotter, F. Nori, and L. Yang, Nat. Mater. **18**, 783 (2019).
[28] S. D. Gupta, N. Ghosh, and A. Banerjee, *Wave Optics: Basic Concepts and Contemporary Trends* (CRC Press, Boca Raton, 2015).
[29] R. Shankar, *Principles of Quantum Mechanics* (Springer Science & Business Media, Heidelberg, 2012).
[30] J. W. Goodman, *Introduction to Fourier Optics* (Roberts and Company, Greenwood Village, 2005).
[31] J. B. Götte and M. R. Dennis, Opt. Lett. **38**, 2295 (2013).
[32] R. C. Jones, J. Opt. Soc. Am. **38**, 671 (1948).
[33] N. Modak, A. BS, A. K. Singh, and N. Ghosh, Phys. Rev. A **103**, 053518 (2021).
[34] Q.-h. Wang, Philos. Trans. R. Soc. A **371**, 20120045 (2013).
[35] Q.-h. Wang, S.-z. Chia, and J.-h. Zhang, J. Phys. A: Math. Theor. **43**, 295301 (2010).
[36] K. Y. Bliokh, F. J. Rodríguez-Fortuño, F. Nori, and A. V. Zayats, Nat. Photonics **9**, 796 (2015).
[37] F. Cardano and L. Marrucci, Nat. Photonics **9**, 776 (2015).
[38] W. Zhang, Y. Wang, D. Xu, and H. Luo, Phys. Rev. A **107**, 043502 (2023).
[39] R. M. Azzam, J. Opt. Soc. Am. A **33**, 1396 (2016).
[40] P. W. Milonni and J. H. Eberly, *Laser Physics* (Wiley, New York, 2010).
[41] J. D. Jackson, *Classical Electrodynamics* (Wiley, 1999).
[42] E. Collett, *Polarized Light: Fundamentals and Applications* (Marcel Dekkar, 1993).
[43] N. Ghosh and I. A. Vitkin, J. Biomed. Opt. **16**, 110801 (2011).
[44] J. J. Gil and R. Ossikovski, *Polarized Light and the Mueller Matrix Approach* (CRC Press, Boca Raton, 2022).